Graphene Oxide Gel-Derived, Free-Standing, Hierarchically Porous Carbon for High-Capacity and High-Rate Rechargeable Li-O_2 Batteries

*Zhong-Li Wang, Dan Xu, Ji-Jing Xu, Lei-Lei Zhang, and Xin-Bo Zhang**

Lithium-oxygen (Li-O_2) batteries are one of the most promising candidates for high-energy-density storage systems. However, the low utilization of porous carbon and the inefficient transport of reactants in the cathode limit terribly the practical capacity and, in particular, the rate capability of state-of-the-art Li-O_2 batteries. Here, free-standing, hierarchically porous carbon (FHPC) derived from graphene oxide (GO) gel in nickel foam without any additional binder is synthesized by a facile and effective in situ sol-gel method, wherein the GO not only acts as a special carbon source, but also provides the framework of a 3D gel; more importantly, the proper acidity via its intrinsic COOH groups guarantees the formation of the whole structure. Interestingly, when employed as a cathode for Li-O_2 batteries, the capacity reaches 11 060 mA h g^{-1} at a current density of 0.2 mA cm^{-2} (280 mA g^{-1}); and, unexpectedly, a high capacity of 2020 mA h g^{-1} can be obtained even the current density increases ten times, up to 2 mA cm^{-2} (2.8 A g^{-1}), which is the best rate performance for Li-O_2 batteries reported to date. This excellent performance is attributed to the synergistic effect of the loose packing of the carbon, the hierarchical porous structure, and the high electronic conductivity of the Ni foam.

1. Introduction

The last two decades have witnessed lithium-ion batteries successfully capture the portable electronics market.[1–7] However, when it is proposed to conquer the upcoming markets of electrical transportation (e.g., electric vehicles) and renewable energies (e.g., wind or solar energy), great improvements in energy density are urgently needed. Rechargeable lithium-oxygen (Li-O_2) batteries have recently attracted a great deal of attention because they can theoretically store 5–10 times more energy than current lithium-ion batteries.[8–18] Prototype Li-O_2 batteries typically consist of a lithium-metal anode, an organic electrolyte, and a porous carbon-based cathode exposed to gaseous O_2 during cell operation. Upon discharge, Li^+ reduces molecular O_2 to form insoluble lithium peroxide (Li_2O_2) or lithium oxide (Li_2O) at the cathode, which gradually blocks the electrolyte and oxygen pathways and eventually also limits the rate capability, capacity, and cyclic life of Li-O_2 batteries.[19–21] Therefore, there is an urgent need to design and synthesize a highly effective carbon cathode for high-performance Li-O_2 batteries.

To this end, intensive research effort has been devoted to improving the performance of Li-O_2 batteries by tuning the morphology and structure of the carbon cathode. Different kinds of carbon, including high-surface area carbons,[22–24] mesocellular carbons,[25] carbon nanotube/nanofiber buckypapers,[26] or graphene,[19,27,28] have been used in O_2 electrodes. As a result, a number of important factors contributing to an improved capacity have been partially identified. For example, it is the mesopore volume of carbon, not the surface area, that plays a key role in affecting the discharge capacity. That is to say, the capacity of the oxygen electrode depends on the surface area of the large pores, not the surface area of all of the pores, and, thus, a carbon with a higher pore volume and a larger pore diameter could increase the discharge capacity.[29–32] In addition, all-carbon-nanofiber electrodes and hierarchically porous graphene have also been applied as Li-O_2-battery electrodes and exhibit high-capacity performances.[20,33] Although much progress has been achieved, the practical discharge capacities are still far below the theoretical value and, especially, simultaneously achieving a high capacity and a high rate in Li-O_2 batteries is still a daunting challenge.[34]

Previous studies have focused on the pore structure of the carbon particles themselves, while the effect of their arrangement in the cathode on the performance of Li-O_2 batteries has been ignored considerably. Generally, the porous carbon particles are closely aggregated by a binder in the cathode and such a tight aggregation unavoidably results in a low O_2-diffusion rate and a limited space for Li_2O_2 deposition, which consequently leads to low utilization of the carbon particles and leads further to a low capacity and low-rate capability of Li-O_2 batteries. Therefore, to achieve both a high capacity and a high-rate performance, it is crucial to solve the low utilization of porous carbon and efficient transport of reactants in the cathode.

Dr. Z.-L. Wang, Dr. D. Xu, Dr. J.-J. Xu, L.-L. Zhang, Prof. X.-B. Zhang
State Key Laboratory of Rare Earth Resource Utilization
Changchun Institute of Applied Chemistry
Chinese Academy of Sciences
Changchun, 130022, P. R. China
E-mail: xbzhang@ciac.jl.cn

DOI: 10.1002/adfm.201200403

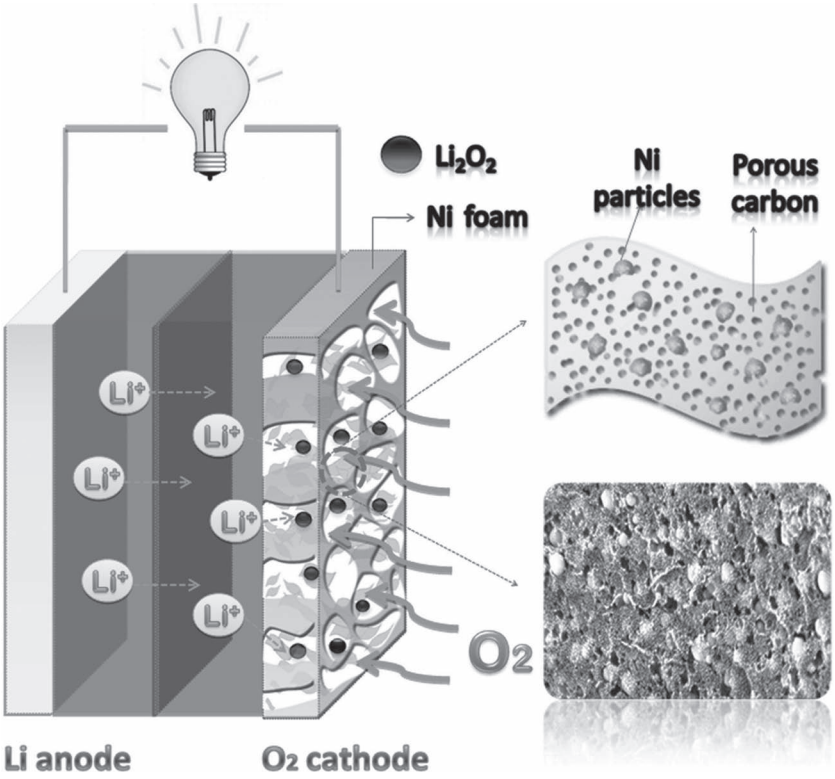

Figure 1. The structure of a rechargeable Li-O_2 battery based on FHPC as the oxygen electrode.

Herein, we firstly propose a strategy to maximize the utilization of porous carbon particles and the transport of reactants by constructing a free-standing, hierarchically porous carbon (FHPC) derived from graphene oxide (GO) gel via a facile and effective in situ sol-gel method, wherein the GO not only acts as a special carbon source, but also provides the framework of a 3D gel; more importantly, the proper acidity via its intrinsic COOH groups plays an important role in the formation of the whole structure.[35–37] Unexpectedly, when employed as the cathode (**Figure 1**), the Li-O_2 battery simultaneously manifests a high specific capacity and an excellent rate capability. This promising performance is attributed to the loose packing of the carbon in the free-standing structure, which provides enough void volume for insoluble Li_2O_2 deposition and increases the efficient utilization of the carbon. Meanwhile, the hierarchically porous structure, including macropores from the nickel foam, and mesopores and micropores from the carbon particles, facilitates O_2 diffusion, wetting of the electrolyte, and mass transport of all the reactants. Furthermore, the FHPC cathode is synthesized directly as a whole part and is free of the conventional complex preparation process of cathodes, and thus could be of great benefit to large-scale fabrication.

2. Results and Discussion

The preparation of the FHPC cathode mainly consists of two steps: the precursor sol solution containing GO, resorcinol (R) and formaldehyde (F) is gelled in situ in nickel foam and then the gelatin is carbonized in a N_2 atmosphere. The basic information of the as-synthesized GO is shown in Figure S1 in the Supporting Information. In this synthesis, the GO acts as not only the special carbon source but also as the framework of a 3D gel during the sol-gel process. Another important role of the GO is that it can provide a weak acid environment by way of the COOH groups of the GO (the pH value of a 1 wt% GO solution is ≈2.3). Due to the weak acid, part of the nickel foam is etched and solved in the sol solution and then forms NiOOH in the precursor gel (Figure S2, Supporting Information). It is the byproduct NiOOH that acts as a special binder between the precursor gel and the nickel foam. In contrast, the gel could hardly coat the nickel foam uniformly when the pH value of the GO was adjusted to 7 by NaOH solution, as is shown in Figure S3 (Supporting Information). In the carbonization process, NiOOH is decomposed into NiO and then reduced by the carbon, forming Ni particles. The consumption of carbon around the Ni particles will produce various pore structures. The existence of Ni particles will not only improve the electrical conductivity, but also adjust the porous structures.

Figure 2a shows the pristine nickel foam with macroporous skeletons. After the in situ synthesis of the porous carbon, a visible black coating in the whole nickel foam was clearly observed (Figure S3, Supporting Information). From the low-magnification scanning electron microscopy (SEM) image (Figure 2b) of the FHPC cathode, the porous carbon particles exhibited a sheet-like morphology due to the introduction of the GO. These porous carbon sheets were loosely packed and were aligned roughly perpendicular to the skeleton surface, which formed free-standing structures, leaving large interconnected tunnels throughout the entire electrode depth. These favorable tunnels should facilitate oxygen transport into the interior of the electrode during the discharge process and provide enough void volume for the discharged products. High-magnification observation (Figure 2c,d) of the carbon sheets revealed that the sheets consisted of numerous small nanoscale pores with diameters between 20 and 100 nm and Ni nanoparticles were embedded in the pores. From the energy-dispersive X-ray (EDX) mapping analysis (Figure S4, Supporting Information), the Ni particles were uniformly distributed in the carbon and the content was about 59 wt%. The thickness of the sheet was about 300 nm (Figure S5, Supporting Information). From the transmission electron microscopy (TEM) image (Figure 2e), a mesoporous (<10 nm) and a microporous texture could be observed in the interior of the sheets. These mesopores and micropores can provide a short ion-transport pathway through the sheet, with a minimized inner resistance. In addition, large Ni particles with diameters ranging from 30 nm to 100 nm were also clearly observed in the carbon substrate, acting as a special binder and conductor of the porous carbon. The N_2-adsorption isotherm and the

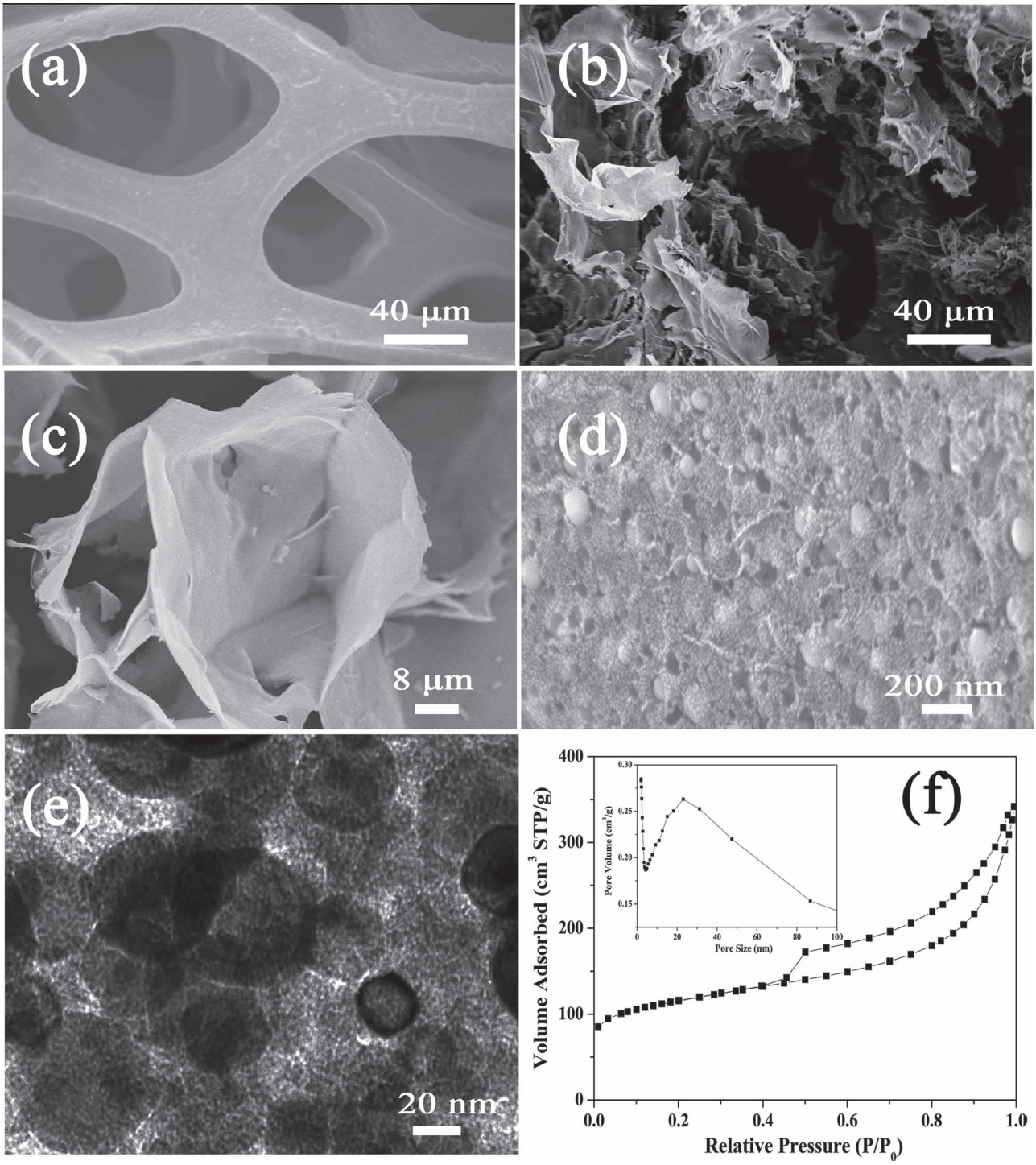

Figure 2. a–d) SEM images of the pristine nickel foam (a) and different magnifications of the as-prepared FHPC electrode (b–d). e) TEM image of FHPC electrode. f) N_2-adsorption-desorption isotherms and pore-size distribution (inset) of the FHPC electrode.

pore-size distribution are shown in Figure 2f. The N_2-adsorption isotherm of the porous-carbon/Ni-particle composite exhibited the combined characteristics of type I/II,[38] with a surface area of 378 $m^2\ g^{-1}$ and a total pore volume of 0.45 $cm^3\ g^{-1}$. The initial region of the isotherms experienced a sharper rise at low P/P_0, indicating the presence of micropores, and the hysteresis loop in the P/P_0 range of ≈0.4–1.0 is indicative of mesoporosity. From the pore-size distribution, it was clearly observed that there were two kinds of pores: micropores (<2 nm) and mesopores with a wide size range (≈5–100 nm), in agreement with

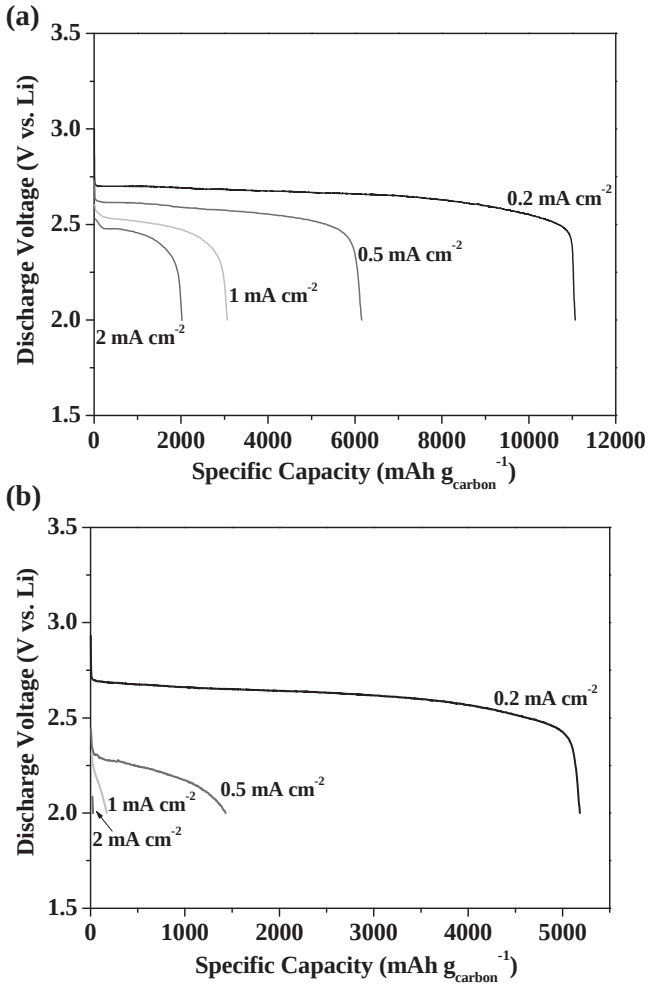

Figure 3. a,b) Discharge curves at different current densities ranging from 0.2 mA cm^{-2} to 2 mA cm^{-2}: FHPC electrode (a) and KB carbon electrode (b).

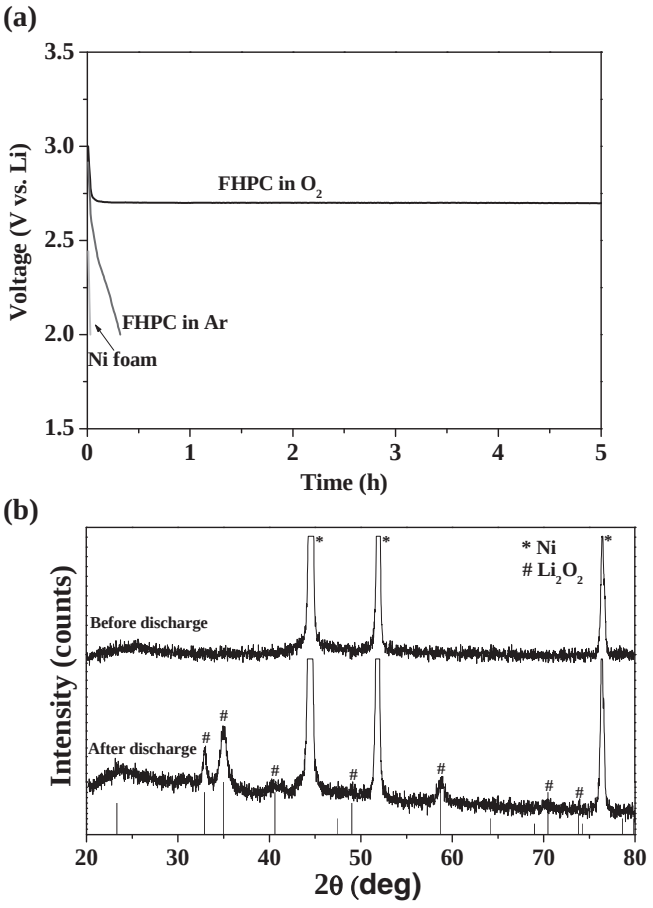

Figure 4. a) Comparable discharge curves of pure nickel foam, the FHPC electrode in Ar and O_2 (the discharge time for the FHPC electrode in O_2, plotted for comparison, is ≈39 h). b) XRD spectra of pristine and discharged FHPC electrodes (0.2 mA cm^{-2}).

the SEM and TEM results. This unique, bimodal, porous structure combined with the macroporous tunnels formed in the framework could be an ideal design for an O_2 electrode. During discharge, the robust large tunnels can function as "highways" to supply oxygen to the interior parts of the cathode, while smaller pores on the carbon sheet are the "exits" to provide the tri-phase (solid-liquid-gas) regions required for oxygen reduction. It should be noted that the presence of NiOOH in the precursor is crucial for the formation of such a porous structure. Without NiOOH in the precursor, the obtained porous carbon had only one kind of small mesopores, which were centered at 4 nm (Figure S6, Supporting Information).

Figure 3a shows the discharge curves of Li-O_2 cells utilizing the FHPC cathode at different current densities and tested in pure oxygen at an initial pressure of ≈2 atm. Interestingly, the discharge capacity at a current density of 0.2 mA cm^{-2} (280 mA g^{-1}) reached 11 060 mA h g^{-1} with a plateau at around 2.64 V, corresponding to the specific energy of 29.2 kW h kg^{-1}. With an increase of the discharge current density, the achieved capacity and operating potential were reduced, due to the internal resistance of the batteries. However, at large current densities of 0.5, 1, and 2 mA cm^{-2}, the discharge capacities were still very high, corresponding to 6150, 3060, and 2020 mA h g^{-1}, respectively. Even increasing the current density to 5 mA cm^{-2}, an acceptable capacity of 370 mA h g^{-1} remained (Figure S7, Supporting Information). This is the best rate performance that has been reported to date for non-aqueous, rechargeable Li-O_2 batteries.[18,33] These results were highly repeatable with multiple parallel test results showing similar capacities under the same test conditions (Figure S8, Supporting Information). To exclude possible electrochemical contributions from lithium-ion intercalation reactions with carbon material, the FHPC cathode was also discharged to 2.0 V in pure argon, as shown in **Figure 4**a. Clearly, the capacity was negligible within the voltage range, which suggests that oxygen reduction by Li^+ was primarily responsible for the discharge capacities of the Li-O_2 cells. Meanwhile, the background discharge capacity of the nickel foam was also negligible, with no discharge-voltage profile. X-ray-diffraction (XRD) (Figure 4b) analysis of the discharged products showed only Li_2O_2, whereas neither Li_2O nor LiOH was detected, which is in agreement with previous studies when ether-based electrolytes were used in Li-O_2 batteries.[39,40]

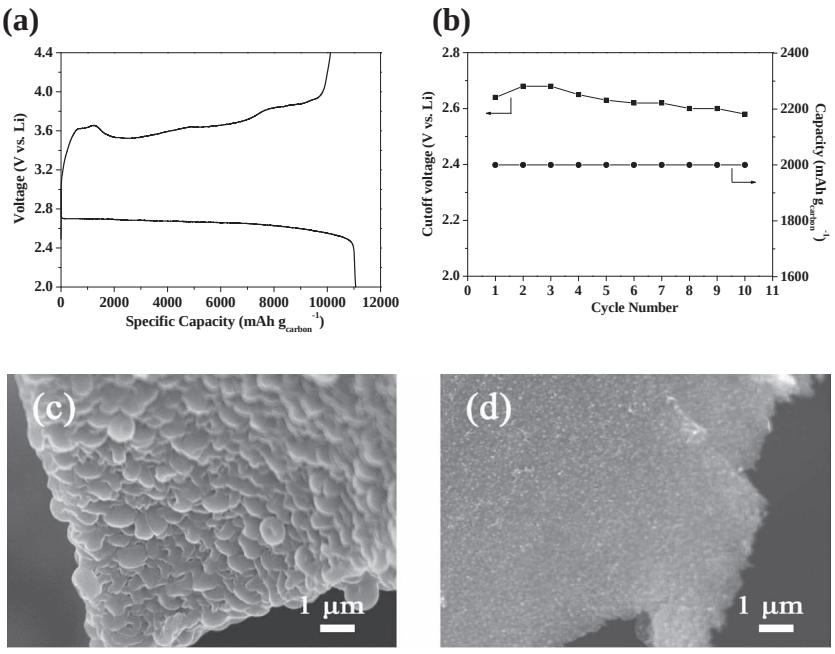

Figure 5. a) Discharge-charge curves of the FHPC-cathode-based Li-O_2 battery at a current density of 0.2 mA cm^{-2}. b) Cycle performance with a restriction of the capacity to 2000 mA h g^{-1} at a current density of 0.5 mA cm^{-2} (circles) and the resulting cut-off voltage of discharge (squares). c,d) SEM images of the FHPC electrode after discharge (c) and discharge-charge (d).

When the mass of discharged product, Li_2O_2, was included, the capacity could still reach a high value of 1054 mA h $g_{discharged}^{-1}$ at a current density of 0.2 mA cm^{-2}, corresponding to an energy density of 2784 W h $kg_{discharged}^{-1}$. Considering the theoretical energy density of pure Li_2O_2 (3215 W h $kg_{Li_2O_2}^{-1}$), the FHPC electrodes that discharged at 0.2 mA cm^{-2} reached roughly 86% of the theoretical value. This energy value represents a nearly 4.6-fold improvement compared with conventional lithium-ion electrodes such as $LiCoO_2$ (600 W h kg^{-1}).[41] In comparison, a conventional O_2 cathode was prepared using commercial KB carbon (EC600JD) with poly(vinylidene fluoride) (PVDF) as a binder. From the discharge curves (Figure 3b), it can be seen that the capacity of the KB carbon was 5180 mA h g^{-1} at a current density of 0.2 mA cm^{-2}, which is only half that of the free-standing porous carbon electrode. As for the rate performance, the KB carbon was not comparable with the novel FHPC cathode. At a current density of 2 mA cm^{-2}, the capacity of the KB carbon cathode was nearly negligible, while that of the FHPC cathode was as high as 2020 mA h g^{-1}. In the highly packed KB carbon cathode, as shown in Figure S9 (Supporting Information), the tightly bonded carbon particles and the binder was composed of a low-porosity electrode, having little space for Li_2O_2 deposition, which would easily block O_2 transportation, leading to a decrease of the electrochemically available surface area. On the contrary, in the free-standing porous carbon cathode, almost all of the surface area of the active carbon could take part in the cell reaction and the obvious loose packing of carbon afforded more abundant O_2- and electrolyte-transportation paths in the electrode.

The galvanostatic charge and discharge behaviors of the Li-O_2 battery at a current density of 0.2 mA cm^{-2} within a voltage window between 2.0 and 4.4 V are shown in **Figure 5**a. During the charge process, it is clear that the charging potential was higher than that on discharge, which is in agreement with previous reports.[32] It was also observed that the charge capacity was close to the discharge capacity, which demonstrates that Li^+ ions from the electrolyte and e^- from the external circuit could combine reversibly with O_2.[42] From the SEM image of the discharged products obtained from the separator side of the cathode (Figure 5c), toroidal-shaped particles with an average diameter of 400 nm were densely aligned on the surface of the porous carbon sheets. Such a high density of Li_2O_2 -particle aggregation indicates further the thoroughness of the electrochemical reactions in the free-standing cathode. A possible formation mechanism of the toroidal-shaped products is that the hexagonal crystal structure of the Li_2O_2 and preferred nucleation on the prismatic crystal faces may give rise to toroidal aggregates of Li_2O_2 nanocrystallites.[43] After charging, the Li_2O_2 particles obviously disappeared (Figure 5d), suggesting a highly reversible process. The cycling performance of the FHPC-cathode-based Li-O_2 cell at a current density of 0.5 mA cm^{-2} is shown in Figure 5b. In the case of a deep discharge with a cut-off voltage of 2.0 V, a relatively higher initial discharge capacity was obtained (Figure 3a). However, the capacity retention remained rather poor, with the discharge capacity dramatically dropping to only 400 mA h g^{-1} after five cycles due to the continuous rise of the resistance. By avoiding a deep discharge and restricting the capacity only to 2000 mA h g^{-1}, the battery exhibited good reversibility for 10 cycles at a current density of 0.5 mA cm^{-2}, as the cut-off voltage did not change dramatically. This result is similar to those reported by Yu et al.[44] and Cui et al.[45] After cycling, the porous carbon was still anchored on the nickel foam (Figure S10, Supporting Information), which illustrates the high stability of the FHPC electrodes. According to reports by Bruce and co-workers, the biggest obstacle for cycling in Li-O_2 batteries is the decomposition of the electrolyte during the charge-discharge process.[40,46,47] Although novel electrolytes require further exploration for better cycling performance, the FHPC cathodes exhibit a promising option for O_2 cathodes in Li-O_2 batteries.

The electrochemical activity of the Ni particles in the cathode was investigated separately. Pure Ni particles (with only a little carbon) were synthesized by using nickel foam modified with $Ni(OH)_2$ as a substrate. Superfluous $Ni(OH)_2$ will have consumed most of carbon during the conversion into Ni particles. From the SEM image shown in Figure S11 (Supporting Information), it can be seen that the carbon nanosheets decreased greatly and the Ni particles became the dominant component in the porous structure, compared with the carbon/Ni-particle composite sheets, while the particle sizes in the two structures were similar (Figure S11c, Supporting Information). Such a Ni-particle cathode was assembled into a battery and tested

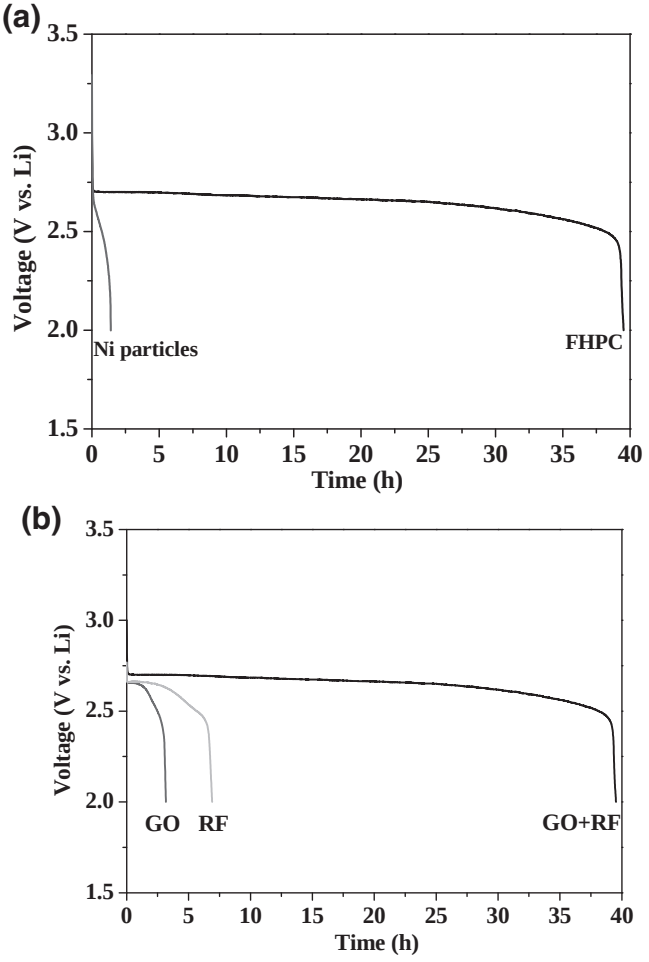

Figure 6. a) Comparable discharge curves of Ni particles and FHPC electrodes. b) Comparable discharge curves of electrodes synthesized from different precursors (GO, RF, and GO + RF).

under the same conditions with the FHPC cathode. As shown in **Figure 6**a, it was clearly observed that the discharge time of the Ni particles was almost negligible compared with that of the carbon/Ni-particle composites, which indicates that Ni particles have no electrochemical activity in Li-O_2 batteries and the capacity from the Ni particles is negligible. Another interesting experiment can illustrate the above conclusion further. When GO and resorcinol/formaldehyde (RF) were used as precursors separately, the obtained products had different components: the products from the GO mainly contained Ni particles (Figure S12a, Supporting Information) and the products from the RF mainly contained carbon particles (Figure S12b, Supporting Information). From the discharge curves (Figure 6b), it was found that the discharge time of the Ni particles was the shortest among the three samples, suggesting that the carbon was the only active material for the cell reactions. The main role of the Ni particles is in adjusting the porous structure of the carbon sheets and increasing the conductivity, as analyzed above. Therefore, porous carbon is the only active material in the cathode and the calculation of capacity should be based on the mass of the carbon.

3. Conclusions

In summary, free-standing, hierarchically porous carbon derived from GO gel was synthesized successfully by a facile and effective in situ sol-gel method. Without any additional treatment, the obtained products could be directly used as an O_2 cathode and simultaneously displayed excellent a high capacity and a high-rate performance. The maximum specific capacity was as high as 11 060 mA h g^{-1} and, most importantly, a high capacity of 2020 mA h g^{-1} could be obtained even the current density increased by a factor of ten times up to 2 mA cm^{-2} (2.8 A g^{-1}), which is the best rate performance for Li-O_2 batteries reported to date. These encouraging results are due to the unique, free-standing, hierarchically porous structure, which facilitated a continuous oxygen flow in the O_2 electrode and also provided enough void volume for Li_2O_2 deposition. This study highlights the importance of a novel electrode design and opens up a promising strategy to develop highly efficient oxygen electrodes for Li-O_2 batteries. Furthermore, such an optimized carbon-electrode construction is also suitable for supercapacitors, fuel cells, and other energy-storage devices.

4. Experimental Section

Materials and Synthesis: GO was synthesized following a procedure described in the literature.[48] Nickel foam (110 PPI, 420 g m^{-2}) was firstly washed with dilute HCl solution and then cut into electrode disks with a diameter of 1.2 cm and a thickness of 1.4 mm. Nickel foam modified with $Ni(OH)_2$ was obtained by immersing washed nickel foam in a growth solution containing $Ni(NO_3)_2$ and NH_4NO_3 for 6 h at 90 °C.[49] The FHPC electrodes were prepared using the traditional organic sol-gel method.[50] In a typical preparation process, a GO (4.5 mL, 1 wt%) solution was dispersed by sonication for 4 h, and then a resorcinol (120 mg)/formaldehyde solution (36 wt%, 180 mg), and a sodium carbonate catalyst (1 mg) were added. The amount of resorcinol and formaldehyde (RF solids) was about 4 wt%. After stirring for 2 h, the sol-gel mixture was dropped into the nickel-foam disks and then transferred to glass molds, sealed, and cured in an oven at 85 °C for 48 h. The water in the resulting gel was removed from the pores of the gel network by a freeze-drying technology. The dry gel embedded in the nickel foam was carbonized in N_2 at 800 °C for 2 h and the obtained products were FHPC electrodes that could be directly used as the cathodes of Li-O_2 batteries. The mass of carbon in the nickel foam was measured by sonication of the FHPC electrode and etching of the Ni particles with HCl solution. On average, each electrode had 0.8 mg of carbon.

Electrochemical Evaluation: Electrochemical experiments were carried out using a Swagelok cell. The cells were prepared inside a glove box under an argon atmosphere, using a clean lithium-metal disk as the anode, a glass-fiber separator, and the FHPC electrode as the cathode. The electrolyte was 1 M lithium bis(trifluoromethanesulfonyl)imide (LITFSI) in 1,2-dimethoxyethane (DME). The salt and solvent used in the electrolyte were all of battery grade. The cell was connected to an oxygen balloon and the gas was exchanged with pure O_2 three times. The cells were rested at open circuit for ≈2–8 h before testing (large current densities need a long rest time). The charge-discharge measurements were carried out using a Land battery system at a constant current density in a voltage range of 2.0–4.4 V versus Li/Li^+. Note that, unless otherwise declared, all of the capacities and current densities reported here were calculated on the basis of the total weight of carbon in the O_2 electrode.

Supporting Information

Supporting Information is available from the Wiley Online Library or from the author.

Acknowledgements

This work was financially supported by the 100 Talents Programme of The Chinese Academy of Sciences, the National Program on Key Basic Research Project of China (973 Program, Grant No. 2012CB215500), the National Natural Science Foundation of China (Grant No. 21101147), and the Jilin Province Science and Technology Development Program (Grant No. 20100102 and 20116008).

Received: February 9, 2012
Published online: May 18, 2012

[1] P. G. Bruce, S. A. Freunberger, L. J. Hardwick, J. M. Tarascon, *Nat. Mater.* **2012**, *11*, 19.
[2] B. Wang, J. S. Chen, H. B. Wu, Z. Wang, X. W. Lou, *J. Am. Chem. Soc.* **2011**, *133*, 17146.
[3] Y. M. Sun, X. L. Hu, J. C. Yu, Q. Li, W. Luo, L. X. Yuan, W. X. Zhang, Y. H. Huang, *Energy Environ. Sci.* **2011**, *4*, 2870.
[4] L. Zhao, Y. S. Hu, H. Li, Z. X. Wang, L. Q. Chen, *Adv. Mater.* **2011**, *23*, 1385.
[5] W. M. Zhang, X. L. Wu, J. S. Hu, Y. G. Guo, L. J. Wan, *Adv. Funct. Mater.* **2008**, *18*, 3941.
[6] X. P. Gao, H. X. Yang, *Energy Environ. Sci.* **2010**, *3*, 174.
[7] F. Y. Cheng, J. Liang, Z. L. Tao, *J. Chen Adv. Mater.* **2011**, *23*, 1695.
[8] K. M. Abraham, Z. Jiang, *J. Electrochem. Soc.* **1996**, *143*, 1.
[9] J. Read, *J. Electrochem. Soc.* **2002**, *149*, A1190.
[10] T. Ogasawara, A. Debart, M. Holzapfel, P. Novak, P. G. Bruce, *J. Am. Chem. Soc.* **2006**, *128*, 1390.
[11] A. Debart, A. J. Paterson, J. Bao, P. G. Bruce, *Angew. Chem. Int. Ed.* **2008**, *47*, 4521.
[12] Y. C. Lu, Z. C. Xu, H. A. Gasteiger, S. Chen, K. Hamad-Schifferli, Y. Shao-Horn, *J. Am. Chem. Soc* **2010**, *132*, 12170.
[13] G. Girishkumar, B. McCloskey, A. C. Luntz, S. Swanson, W. Wilcke, *J. Phys. Chem. Lett.* **2010**, *1*, 2193.
[14] Y. C. Lu, Hubert H. A. Gasteiger, Y. Shao-Horn, *J. Am. Chem. Soc.* **2011**, *133*, 19048.
[15] B. D. McCloskey, R. Scheffler, A. Speidel, D. S. Bethune, R. M. Shelby, A. C. Luntz, *J. Am. Chem. Soc.* **2011**, *133*, 18038.
[16] J. S. Lee, S. T. Kim, R. Cao, N. S. Choi, M. Liu, K. T. Lee, J. Cho, *Adv. Energy Mater.* **2011**, *1*, 34.
[17] Y. M. Cui, Z. Y. Wen, Y. Liu, *Energy Environ. Sci.* **2011**, *4*, 4727.
[18] Y. F. Wang, D. Zheng, X. Q. Yang, D. Y. Qu, *Energy Environ. Sci.* **2011**, *4*, 3697.
[19] E. Yoo, H. Zhou, *ACS Nano* **2011**, *5*, 3020.
[20] J. Xiao, D. H. Mei, X. L. Li, W. Xu, D. Y. Wang, G. L. Graff, W. D. Bennett, Z. M. Nie, L. V. Saraf, I. A. Aksay, J. Liu, J. G. Zhang, *Nano Lett.* **2011**, *11*, 5071.
[21] S. S. Zhang, D. Foster, J. Read, *J. Power Sources* **2010**, *195*, 1235.
[22] J. Xiao, D. H. Wang, W. Xu, D. Y. Wang, R. E. Williford, J. Liu, J. G. Zhang, *J. Electrochem. Soc.* **2010**, *157*, A487.
[23] S. D. Beattie, D. M. Manolescu, S. L. Blair, *J. Electrochem. Soc.* **2009**, *156*, A44.
[24] C. K. Park, S. B. Park, S. Y. Lee, H. Lee, H. Jang, W. I. Cho, *Bull. Korean Chem. Soc.* **2010**, *31*, 3221.
[25] X. H. Yang, P. He, Y. Y. Xia, *Electrochem. Commun.* **2009**, *11*, 1127.
[26] G. Q. Zhang, J. P. Zheng, R. Liang, C. Zhang, B. Wang, M. Hendrickson, E. J. Plichta, *J. Electrochem. Soc.* **2010**, *157*, A953.
[27] Y. L. Li, J. J. Wang, X. F. Li, D. S. Geng, R. Y. Li, X. L. Sun, *Chem. Commun.* **2011**, 9438.
[28] B. Sun, B. Wang, D. W. Su, L. Xiao, H. Ahn, G. X. Wang, *Carbon* **2012**, *50*, 727.
[29] X. M. Ren, S. S. Zhang, D. T. Tran, J. Read, *J. Mater. Chem.* **2011**, *21*, 10118.
[30] M. Mirzaeian, P. J. Hall, *Electrochim. Acta* **2009**, *54*, 7444.
[31] C. Tran, X. Q. Yang, D. Y. Qu, *J. Power Sources* **2010**, *195*, 2057.
[32] S. R. Younesi, S. Urbonaite, F. Björefors, K. Edström, *J. Power Sources* **2011**, *196*, 9835.
[33] R. R. Mitchell, B. M. Gallant, C. V. Thompsona, Y. Shao-Horn, *Energy Environ. Sci.* **2011**, *4*, 2952.
[34] Y. C. Lu, D. G. Kwabi, K. P. C. Yao, J. R. Harding, J. Zhou, L. Zuind, Y. Shao-Horn, *Energy Environ. Sci.* **2011**, *4*, 2999.
[35] L. H. Wang, K. Y. Pu, J. Li, X. Y. Qi, H. Li, H. Zhang, C. H. Fan, B. Liu, *Adv. Mater.* **2011**, *23*, 4386.
[36] X. Huang, X. Y. Qi, F. Boey, H. Zhang, *Chem. Soc. Rev.* **2012**, *41*, 666.
[37] D. C. Wei, Y. Q. Liu, *Adv. Mater.* **2010**, *22*, 3225.
[38] D. W. Wang, F. Li, M. Liu, G. Q. Lu, H. M. Cheng, *Angew. Chem. Int. Ed.* **2008**, *47*, 373.
[39] C. O. Laoire, S. Mukerjee, E. J. Plichta, M. A. Hendrickson, K. M. Abraham, *J. Electrochem. Soc.* **2011**, *158*, A302.
[40] S. A. Freunberger, Y. H. Chen, N. E. Drewett, L. J. Hardwick, F. Bard, P. G. Bruce, *Angew. Chem. Int. Ed.* **2011**, *50*, 8609.
[41] H. Chen, M. Armand, G. Demailly, F. Dolhem, P. Poizot, J. M. Tarascon, *ChemSusChem* **2008**, *1*, 348.
[42] Y. G. Wang, H. S. Zhou, *Energy Environ. Sci.* **2011**, *4*, 1704.
[43] R. Black, S. H. Oh, J. H. Lee, T. Yim, B. Adams, L. F. Nazar, *J. Am. Chem. Soc.* **2012**, *134*, 2902.
[44] D. Zhang, Z. Fu, Z. Wei, T. Huang, A. Yu, *J. Electrochem. Soc.* **2010**, *157*, A362.
[45] S. M. Dong, X. Chen, K. J. Zhang, L. Gu, L. X. Zhang, X. H. Zhou, L. F. Li, Z. H. Liu, P. X. Han, H. X. Xu, J. H. Yao, C. J. Zhang, X. Y. Zhang, C. Q. Shang, G. L. Cui, L. Q. Chen, *Chem. Commun.* **2011**, 11291.
[46] S. A. Freunberger, Y. H. Chen, Z. Q. Peng, J. M. Griffin, L. J. Hardwick, F. Barde, P. Novak, P. G. Bruce, *J. Am. Chem. Soc.* **2011**, *133*, 8040.
[47] Z. Q. Peng, S. A. Freunberger, L. J. Hardwick, Y. H. Chen, V. Giordani, F. Barde, P. Novak, D. Graham, J. M. Tarascon, P. G. Bruce, *Angew. Chem. Int. Ed.* **2011**, *50*, 6351.
[48] D. C. Marcano, D. V. Kosynkin, J. M. Berlin, A. Sinitskii, Z. Z. Sun, A. Slesarev, L. B. Alemany, W. Lu, J. M. Tour, *ACS Nano* **2010**, *4*, 4806.
[49] Y. Wang, D. X. Cao, G. L. Wang, S. S. Wang, J. Y. Wen, J. L. Yin, *Electrochim. Acta* **2011**, *56*, 8285.
[50] M. A. Worsley, P. J. Pauzauskie, T. Y. Olson, J. Biener, J. H. Satcher Jr., T. F. Baumann, *J. Am. Chem. Soc.* **2010**, *132*, 14067.